Detecting Heavy Metals in Solution Using Electronic-Tongue 3 REDOX Water Quality Sensors

Gregory M. Kuhlman[1,2], Didier Keymeulen, and Martin G. Buehler
Jet Propulsion Laboratory, California Institute of Technology, 4800 Oak Grove Drive, Pasadena, CA 91109, 818-393-0951,
gregory.m.kuhlman@jpl.nasa.gov
and
Samuel P. Kounaves, Department of Chemistry. Tufts University

Abstract—This paper describes results obtained from the E-Tongue 3 apparatus used to characterize residual contaminates in water. This apparatus is intended for use in water quality measurements for the ISS (International Space Station). The apparatus contains nine planar electrochemical cells and a conductivity sensor. Detection of contaminate ions in solution uses ASV (Anodic Stripping Voltammetry) with a detection limit in the 10 μM range. A linear calibration curve was achieved using Zn Pb, Cu, and Mn cations. A robust method for identifying electroactive species is presented and uses the Savitzky-Golay second derivative method.

TABLE OF CONTENTS

1   INTRODUCTION

This paper extends the work reported at last year's IEEE Aerospace conference where the design principles for the fabrication of Electronic Tongue No. 2 [1]. This paper describes measurements and data analysis obtained from REDOX cells found on E-Tongue 3 sensor seen in Fig. 1. The electroactive species were characterized using Anodic Stripping Voltammetry (ASV) [2]

The goal of this effort is to develop long-life sensors for water quality measurements for use on the International Space Station Alpha and Martian habitates. A list of the trace elements found in drinking water is given in Table 1. The allowable contaminant limits are given in mg/L and μM. The table also lists standard electrochemical series potential, E°, and the ASV measurement method.

This effort is an outgrowth of the 25-cm^3 electrochemical cell developed for the MECA (Mars Environmental Compatibility Assessment) project [3] which included 20 prefabricated Ion Selective Electrodes, a conductivity sensor, a temperature sensor and an oxidation reduction potential sensor. Traditional electrochemical sensors are fabricated at the end of a pencil-like cylindrical tube. Such sensors cannot be configured easily in a multi-sensor array nor can they be miniaturized.
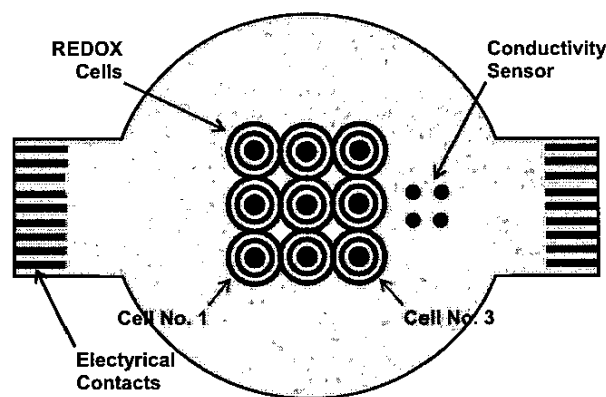

Figure 1. Schematic view of E-Tongue 3 4-cm (1.57-inch) diameter ceramic substrate with nine REDOX cells and conductivity sensor on the topside and on the backside a thermometer and heater.

The basic ASV response curves are shown in Fig. 2. These curves were obtained from the REDOX cells are used to establish the calibration curves which is discussed in a later section. The ASV curves shown in Fig. 2 were obtained from sequentially exposure of the REDOX cells to 100 μM $ZnSO_4$, $CuSO_4$, $PbCl_2$, and $MnSO_4$. The data were acquired using ASV at the stated deposition time, T_{dep} and a scan rate of S = 20 mV/s. The voltage wave, used in these experiments, is described in detail a later section.

Table 1. Drinking Water Trace Contaminates

Name	Com- pound	Molecular Weight g/mol	EPA mg/L	EPA μM	E^o V [HCP]
Inorganic Chemicals					
Zinc	Zn	65.38	70	1070.664	-0.762
Barium	Ba	137.33	7.5	54.613	-2.912
Nickel	Ni	58.69	1	17.039	-0.257
Lead	Pb	207.2	1.5	7.239	-0.126
Arsenic	As	75.9216	0.5	6.586	-0.608
Chromium	Cr	51.996	0.33	6.347	-0.913
Silver	Ag	107.868	0.3	2.781	-0.8
Selenium	Se	78.96	0.16	2.026	-0.924
Antimony	Sb	121.75	0.19	1.561	-0.51
Beryllium	Be	9.01218	0.01	1.110	-1.847
Cadmium	Cd	112.41	0.05	0.445	-0.403
Thallium	Tl	204.383	0.02	0.098	-1.899
Mercury	Hg	200.59	0.009	0.045	0.851
Secondary Standards (Aesthetics)					
Chloride	Cl	35.45	250	7052.186	1.358
Sulfate	SO4	96.07	250	2602.269	0.172
Copper	Cu	63.54	1	15.738	0.153
Iron	Fe	55.85	0.3	5.372	-0.447
Manganese	Mn	24.32	0.05	2.056	-1.185

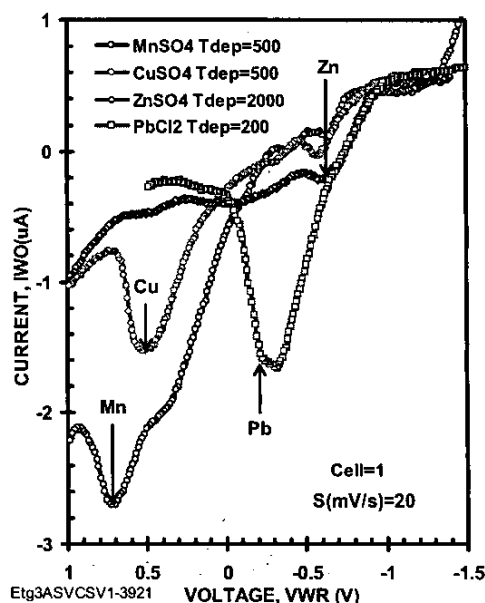Figure 2. ASV data for four heavy metal ions measured with at 100-μM concentration. The sweep rate was 20 mV/s and the deposition time, Tdep, varied from 200 to 2000 s depending on the ion.

In simple terms, the voltage is maintained at a negative potential for a time, T_{dep} and scanned to a positive voltage at a rate of 20 mV/s. The negative potential attracts positively charged cations to the working electrode of the electrochemical cell.

Once the potential is scanned toward a positive potential, the electroactive species are stripped from the electrode at a potential that is near the REDOX potential, E^0. At this potential, the neutral deposited ions become oxidized and re-enter the solution. The oxidation of the ions deposits electrons on the working electrode which creates a current that is detected by an ammeter. The measured potential and current form the response seen in Fig. 2.

A schematic of the ASV process is seen in Fig. 3. Here an electrochemical cell has a working electrode (WE), a reference electrode (RE), and an auxiliary electrode (AE) connected to external circuitry consisting of a battery, an ammeter, and two voltmeters. The potential measured between the WE and RE is the voltage VWR and the potential measured between the AE and RE is the voltage VAR.

a) Reduction/Deposition
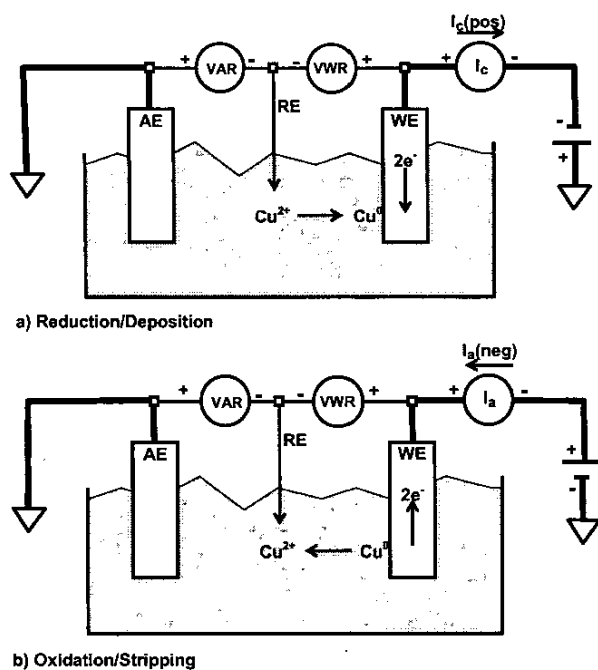

b) Oxidation/Stripping

Figure 3. Schematic of Anodic Stripping Voltammetry (ASV) deposition/stripping steps. Bold lines indicate the main current flow in external circuit.

In Fig. 3a, positively charged cations are attracted to the WE where the ions are reduced by acquiring electrons. This contributes to a cathodic current, I_c, which is positive as it passes through the ammeter. The deposition process takes a time called, T_{ASVdep}.

After the deposition time, the direction of the scanned potential is reversed and proceeds from a negative to positive potential. The ions enter solution as depicted in Fig. 3b. When leaving the WE, the ions loose their electrons to the WE and this contributes to an anodic current, I_a, which is negative as it passes through the ammeter.

The ions enter the solution close to their REDOX potential, E^0. The REDOX potential is known from the Electrochemical Series [4]. Thus, a likely chemical identity of an ion can be determined. The uncertainty in the identification is due to lack of uniqueness of the REDOX potential. However, additional knowledge of the likely candidate ions can rule out many low likelihood ions.

2 E-TONGUE SENSORS

The substrate used in this experiment is seen in Fig. 4. It contains nine REDOX cells, a conductivity sensor, a thermometer and a heater. Only the REDOX cells are discussed in this paper.
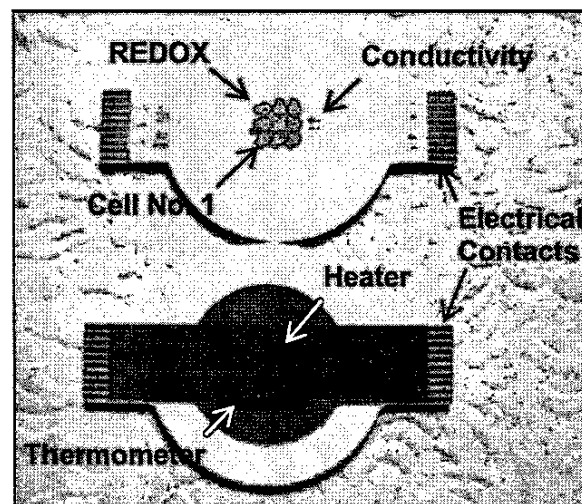

Figure 4. Ceramic-based REDOX and conductivity sensors are shown in the top view and the heater and thermometer are shown in the bottom view. The long dimension is 6.1 cm.

The substrates are fabricated using hybrid microelectronic fabrication methods where each layer is screen printed onto the ceramic substrate and fired in an air atmosphere at 850°C. The substrate is 1.25-mm thick and is 96% alumina. Electrical contact to the sensors is achieved by using 0.25-mm vias created using laser drilling. The vias are made conducting by screen printing a metal layer that is drawn through the via using a mild vacuum. The vias are connected to wires screen printed on the underside of the substrate and connected to electrical contacts. The bottom wires are protected by a dielectric layer. This substrate contains 27 electrical contacts.

Photomicrographs of the REDOX cells are shown in Figs. 4a and 4b. All three electrodes (WE, RE, and AE) were formed from screen printed gold. The WE diameter is 0.75 mm. The RE is 0.25 mm wide and separated from the WE and AE by 0.25 mm. The inner diameter of the AE is 2.75-mm. As far as the authors know, this design is unique in that it is planar and has a common AE that is shared with all nine cells.
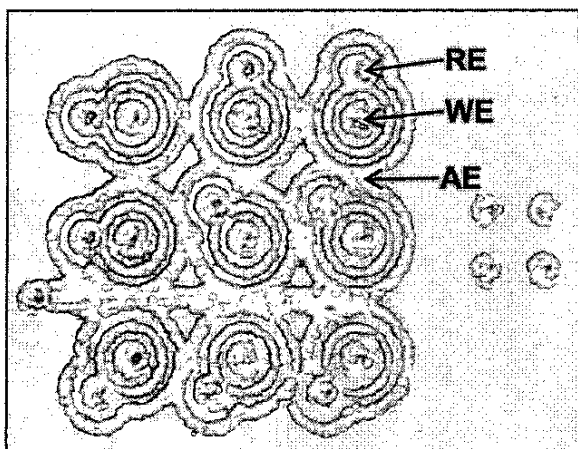
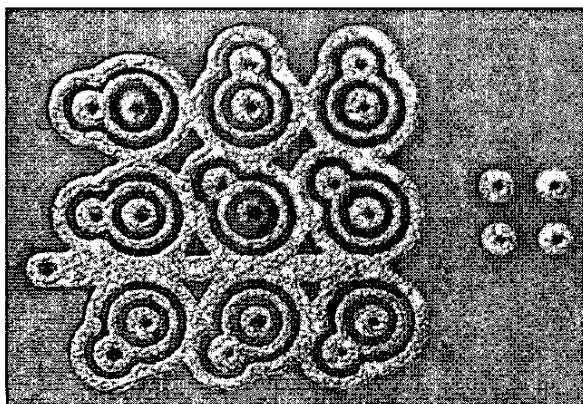Figure 4a. Photomicrograph of E-tongue 3 sensors prior to deposition.

Fig. 4b. Zn deposition visible on WE of cells 5 and 7.

The ion stream lines for the REDOX cell is visualized as a three-dimensional flow that starts at the WE and terminates on the AE. The RE senses the potential, VWR, between the WE and RE. VWR is the potential drop across both the double layer formed at the WE and the solution series resistance between the WE and RE.

The E-Tongue 3 electrochemical cells allow a visualization of the deposition process. The as-fabricated cells prior to deposition are shown in Fig. 4a. Notice that the actual cells in Fig. 4 differ from the schematic shown in Fig. 1. That is the actual RE ring is connected to a disk that is used to accommodate the RE via.

After deposition and prior to stripping, metal deposition can be seen decorating Cells 5 and 7 in Fig. 4b. This demonstrates another important aspect of the array. That is certain cells can be targeted for deposition with all other cells turned off. This is an important attribute of the electronic circuitry discussed later. In many cases, the visualization capabilities are quite striking.

3 APPARATUS

The electronics used to measure the REDOX and conductivity sensors is shown in Figs. 5a and 6. The apparatus seen in Fig. 5a has a ceramic substrate housed in a polycarbonate flow through chamber. Each end of the ceramic substrate are connected to the electronics board through flex cables. The electronics is located on the printed wiring board. This circuitry is controlled by a PC-Card (NI6533) inserted into a laptop computer. This apparatus fits on the stage of a Zeiss Axioplan fitted with a 100X objective [5].
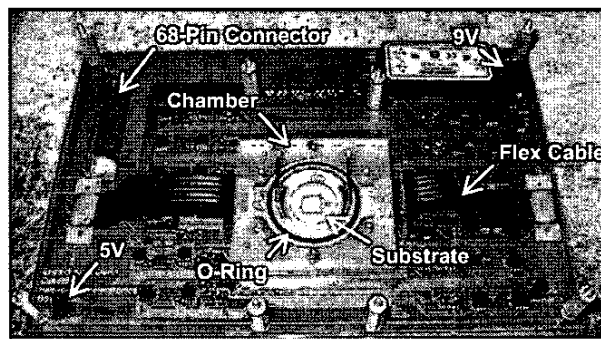

Figure 5a. E-Tongue-3 apparatus with the electrochemical cells housed in a flow-through chamber. The ceramic substrate is connected by flex cables to a 14.3 cm x 21.7 cm electronic board.

The chamber is designed with two O-rings. One O-ring is positioned on the top and bottom of the ceramic. A water-tight seal is achieved by clamping the top and bottom polycarbonate portions of the chamber with the six screws visible on the top of the chamber. This provides a water tight seal and eliminates bending stress on the ceramic substrate. In addition, the flex cables also function to relieve stress on the ceramic. To date non of the ceramic substrates have broken.

The data acquired from this apparatus were obtained using an open chamber as opposed to a closed chamber configuration. The closed chamber has a 0.15-mm thick cover glass located 0.50-mm above the ceramic substrate. This provides about a μL sample volume above the sensors. When the cover glass is removed, the sample volume is about 1 mL. This is important in that the sample volume for the closed chamber is a restricted source from which to draw ions for deposition on the working electrode. The sample volume for the open chamber is about four times larger than for the closed chamber. Most experiments reported here used the open chamber.
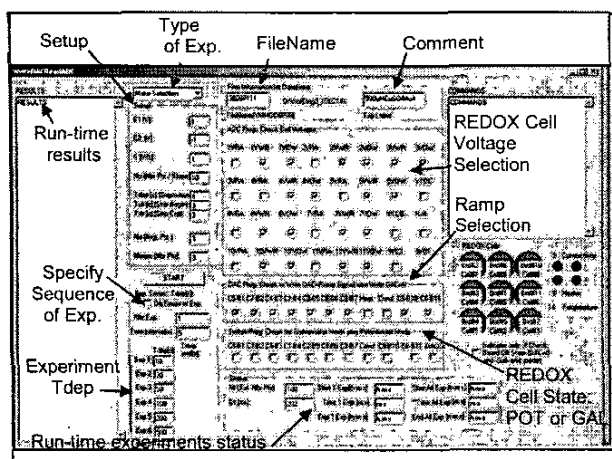
f1363_8.doc - 4

Figure 5b. User interface controlling the E-Tongue-3 apparatus allowing automatic sequencing of experiments each with a different deposition time.

A graphical user interface (GUI), seen in Fig. 5b, was developed to allow users to specify the type and parameters of the experiment(s). The *Type of Exp*eriment is selected through the combo box interface showing CSV&ASV. The experiment parameters are defined in the *Setup* window including the voltage limits (E_1 and E_2), scan rate (S), deposition time (Tdep), number of samples/slope (Np) and average (Na) points/sample. The interface also allows the user to select the REDOX cells used for the experiment and the ones in a neutral electrochemical state using the *ADC Prog. window*. In the *DAC Prog.* window, the cells are selected to receive the DAC ramp signal. In the *Switch Prog.* window, the mode potentiostat or galvanostat is selected. Once the experiment is started, the interface shows the *Status* of the experiment and the execution time. This information is important since some experiments can take several hours. The graphical user interface (GUI) also allows the user to perform eight experiments automatically each with a different Tdep. The number of experiments and Tdep parameters for each experiment are defined in the *Exp. Series: Tdep* window. The interface also allows the user to monitor results through the *Results* window while the experiments are running.

The REDOX circuitry shown in Fig. 6 is a dual potentiostat/galvanostat that is replicated for each of the nine electrochemical cells. The current through the cell is determined by the instrumentation amplifier, IA2, and the resistor R_0; that is $I = -VOW/R_0$. Each REDOX cell has its own DAC (Digital-to-Analog-Converter) and this means that the current through each REDOX cell is independent. Each cell can then be configured as a potentiostat or galvanostat by closing and opening the appropriate switches. This is important for cells that are not in use; these cells are configured as galvanostats with zero current.

Evidence of this function is seen in Fig. 4b where only cells 5 and 7 have deposited metal.
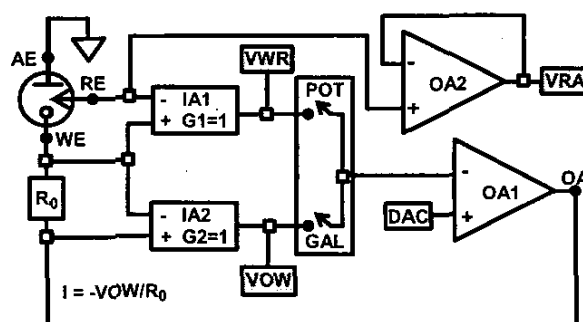
Figure 6. E-Tongue 3 circuitry.

The key feature of this design is the shared AE; this electrode is in common all the REDOX cells. This feature reduces the number of pins or wires from the array of cells. In addition, the grounded AE provides an intrinsic isolation of each cell in that their electric fields do not interfere. In addition, the grounded AE provides a ground plane for the entire cell that acts like an electrical shield that reduces noise. The common, grounded AE is a unique feature of this REDOX cell design.

In the potentiostat mode, the POT switch is closed and VWR is set equal to the DAC voltage. Thus, in this mode, the DAC voltage is forced across the WE and RE by Operation Amplifier #1 (OA1) which adjusts the current using its feedback property. In the galvanostat mode, the GAL switch is closed and the DAC voltage is forced across VOW. That is, the current through the cell is forced and the VWR adjusted by OA1.

4   POTENTIAL WAVEFORM

The waveform used with these measurements is shown in Fig. 7. This voltage ramp is applied to the DAC terminal of the circuitry shown in Fig. 6. This wave form is a departure from wave forms used in previous E-Tongues in that there are no voltage jumps between the ramp segments. This has eliminated current spiking which were not in control when acquiring data using E-Tongue 1 and 2. In addition, this waveform is directed at detecting positively charged cations. That is the first part of the wave, where the voltage is positive during T_{CSVdep}, rejects cations and tends to clean the electrode.
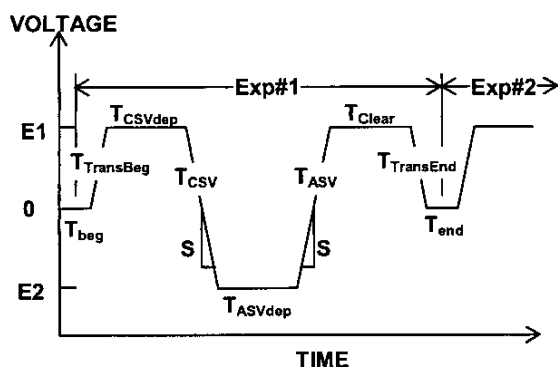
VOLTAGE

Figure 7. Overview of the waveform for the measurements used in this study.

The waveform, shown in Fig. 7, starts at zero volts and transitions to the positive voltage, E1. The voltage remains at E1 for a deposition time, T_{CSVdep}, where CSV is cathodic stripping voltammetry. The voltage then transitions to a negative voltage, E2, during a period T_{CSV}. The voltage remains at E2 for a deposition time, T_{ASVdep}. Finally the wave returns to zero volts after a time T_{clear}. This concludes experiment #1, Exp#1. If called for by the software, experiment #2 then begins. In the current version of the software the following times are identical; that is, $T_{CSVdep} = T_{ASVdep} = T_{clear} = T_{dep}$. The magnitude of the scan rate S is the same for all experiments.

The waves are created using a 16-bit DAC with a resolution of 12-μV resolution. A total of 200 data points are taken between E1 and E2. For a span (E1 – E2) of 2 V each potential step is 10 mV. The measurements were conducted at a stated scan rate, S, and Tdep times which could be programmed from 1 s to 5000 s. The overall measurement time could take as much as 4 hours.

5   SEM ANALYSIS OF E-TONGUE SENSORS

In this section we examine the morphology the ceramic substrate and the screen-printed gold electrodes. We are looking for clues to reproducible electrochemical signals and the subsequent development of electrode cleaning procedures.

5.1   Electrode Morphology

Electrodes are manufactured by screen-printing a gold ink on the ceramic substrate. The gold ink contains gold beads approximately 1 μm in diameter, a glassy fritting material, and an organic binder that is volatilized during the firing process [6]. The ceramic substrate is seen in Fig 8. The rough surface of the alumina is key to allowing the glassy fritting material to adhere to the ceramic during the firing cycle. At the same time the fritting material binds to the gold beads. Thus the electrodes consist of a sandwich with the ceramic at the bottom, the fritting material in between, and gold on top.

Figure 8. SEM photomicrograph of E-tongue 3 sensor. Ceramic material.   SEM conditions: 20 kV, 2000x magnification.
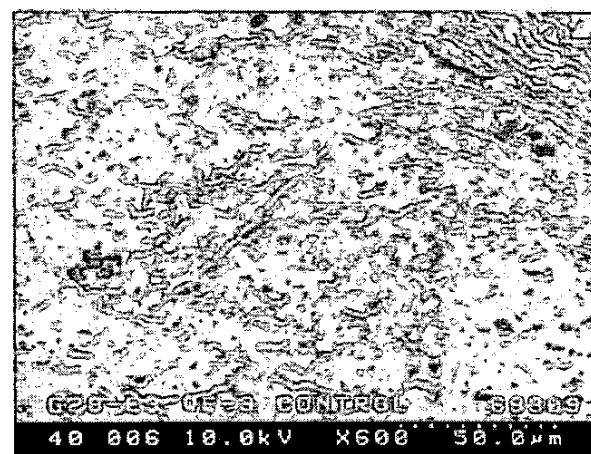

Figure 9. SEM photomicrograph of E-tongue 3 sensor. Virgin Au surface of working electrode. SEM conditions: 10 kV, 600x magnification.

After the gold ink is screen-printed onto the substrate it is allowed to dry at room temperature and then fired at 850°C for 15 minutes. Because there are several different screen printed layers placed on each ceramic, the REDOX electrodes sometimes see as many as 5 or 6 firing cycles at 850°C. Fig. 9 shows a virgin gold electrode.

Each firing cycle re-orders the glassy fritting material and the gold and can coat the electrodes with a glassy layer. We looked for an excess of gold on top of the electrodes and we were pleasantly surprised to find only a small amount of glassy material.

After the gold electrodes were abraded with an eraser, small inclusions were revealed as seen in Fig. 10. The inclusions are most likely from the underlying fritting

f1363_8.doc - 6

368

material that did not attach to the ceramic during the firing process. SEM chemical analysis of the inclusions showed that they are composed of a variety of elements including silicon, lead, oxygen, calcium, cadmium and zinc. These elements are common components of fritting material especially silicon and oxygen.
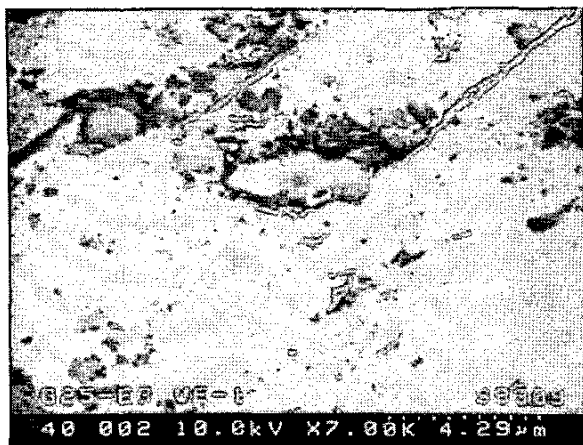

Figure 10. SEM photomicrograph of E-tongue 3 electrode. Surface abrasion reveals inclusions from fritting material in Au working electrode. SEM conditions: 10 kV, 7000x magnification.

Other electrodes were also analyzed. Platinum electrode surfaces appear much more porous and granular than gold surfaces. This is most likely due to a difference in the starting material and not the screen printing technique since both electrodes have been fired equally. Silver electrodes appear to have the same type of rough surface as platinum when screen printed in a similar manner. Gold, platinum and silver have different capabilities in regards to their ability to detect different compounds in solution, but this most likely due to the difference in electrode material and not surface morphology. Most of our Etng 3 analysis were performed with gold electrodes because the data shows the greatest reproducibility.

5.2   Electrode Cleaning Procedure

Before measuring contaminated water, the electrodes are cleaned. During the past six months a number of cleaning procedures were tried. Our latest procedure is as follows. First the raw ceramic substrate is lightly lapped with 2000 grit silicon carbide paper to remove any hillocks remaining after the electrode screen printing process. After an ASV measurement sequence, residual metals are removed from the electrodes using a finishing pad available from 3M (Part 7414). Residue from this process is removed using a cotton swab soaked in a flux remover available from M. G. Chemicals Part 414. The ceramic is given a final cleaning using a cotton swab soaked in IPA (IsoPropyl Alcohol). The residual IPA is removed using a dry cotton swab. If

sterility is needed, the ceramic substrate, polycarbonate chamber and O-ring can be autoclaved.

6   ASV MEASUREMENT

In this section, E-Tongue 3 ASV measurements are used to illustrate:
- Baseline water response
- REDOX cell calibration
- Scan rate dependence
- Open/closed chamber response
- Two species analysis

In the following measurements all the REDOX cell electrodes were gold, the scan rate was 20 mV/s, the deposition times, T_{dep}, are listed in the legend of each figure and the VWR voltage was scanned generally from - 1.5 V to +1V.

6.1   Baseline Water Response

The ASV water response is shown in Fig. 11. The values at -1.5 V indicate the strength of the cathodic currents that exist at the end of the T_{ASVdep} period. The currents seen at - 1.5 V can be explained as follows. For shorter T_{dep} times, the currents at -1.5 V are higher because the displacement current through the cell has not had time to recover from the negative going CSV scan. At longer T_{dep} times, the currents at -1.5 V are smaller, because the current has had time to equilibrate during the T_{ASVdep} period.

The limits on the voltage span are set by the electrolysis of water where hydrogen is generated at negative potentials and oxygen at positive potentials. The voltage span of 2.5 V seen in Fig. 11 is encouraging. A comparison can be made for a platinum electrode where the span is about 1.5 V [7] For positive potentials, gold is limited in Chlorine solutions to about +0.8 V because of the Au-Cl reaction [8].
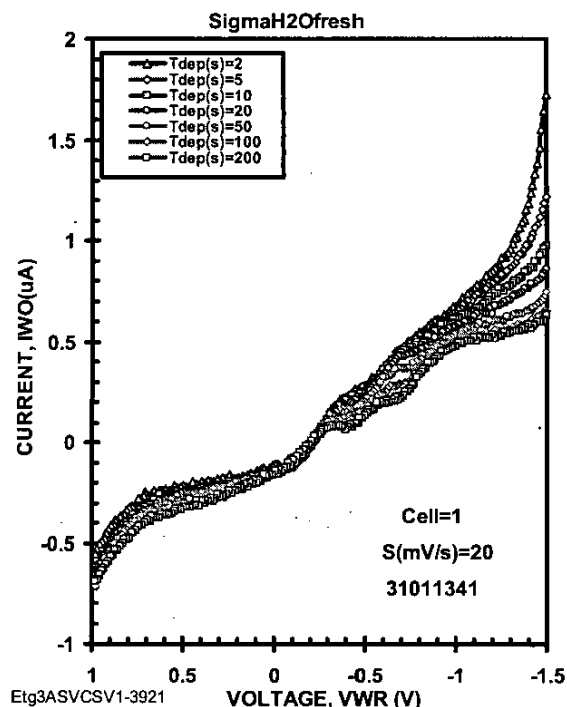
Figure 11. ASV response for Sigmapure water

6.2 REDOX Cell Calibration

The calibration of the instrument was performed using four cations whose electrochemical response lies between the electrolysis limits. The ions used in this calibration procedure were 100 µM of $ZnSO_4$, $PbCl_2$, $CuSO_4$, and $MnSO_4$. The 100 µM concentration was chosen to be close to the detection limits listed in Table 1. The detection of residuals contaminates in water is difficult because the resistance of the water is high. This means that the voltage drop across the solution is much larger than the voltage drop across the double layer at the WE. Nevertheless, in spite of these difficulties, detection at 100 µM has been demonstrated.

Each solution was introduced one at a time into an open sample chamber where the cover glass was removed so the chamber could receive a 1 mL solution. The sweep rate was held constant at 20 mV/s and substrate (No. G41) had gold electrodes. Results for cell number one is shown in Figs. 12 to 15 for seven T_{dep} times shown in the legend of each figure.

The peak currents and voltages are shown in Figs. 12b to 15b. The peak values were extrapolated to zero current where the REDOX potential, E^0_{meas}, was determined. These values provide the measured REDOX potentials shown in Fig. 16.
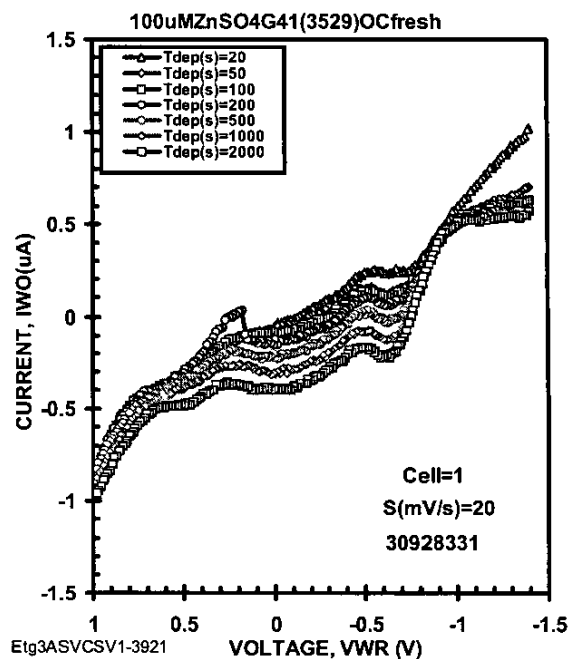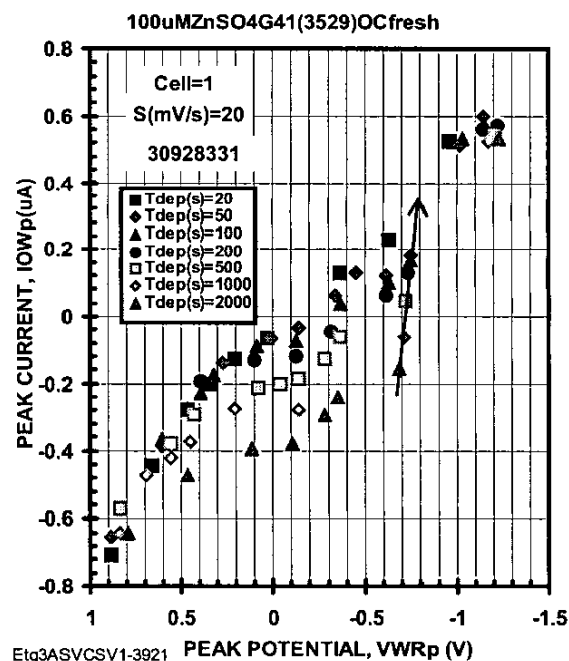

Figure 12a. 100 µM $ZnSO_4$ ASV response.

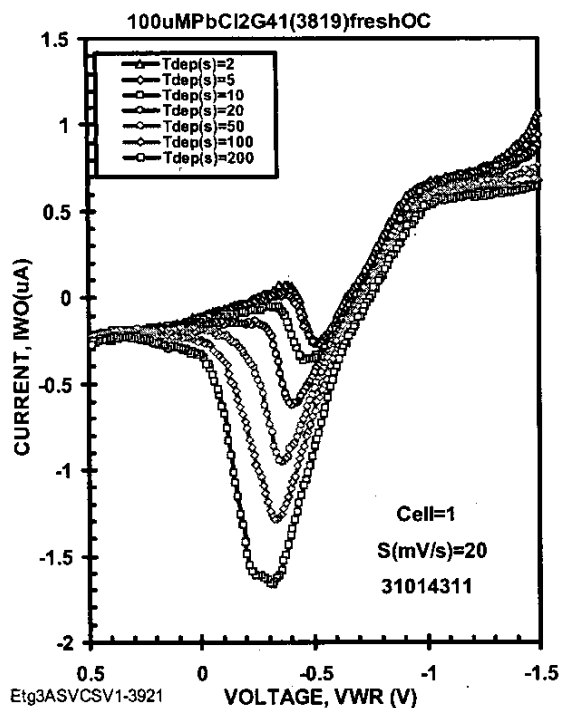Figure 12b. 100 µM $ZnSO_4$ peak response for ASV response seen in Fig. 12a.
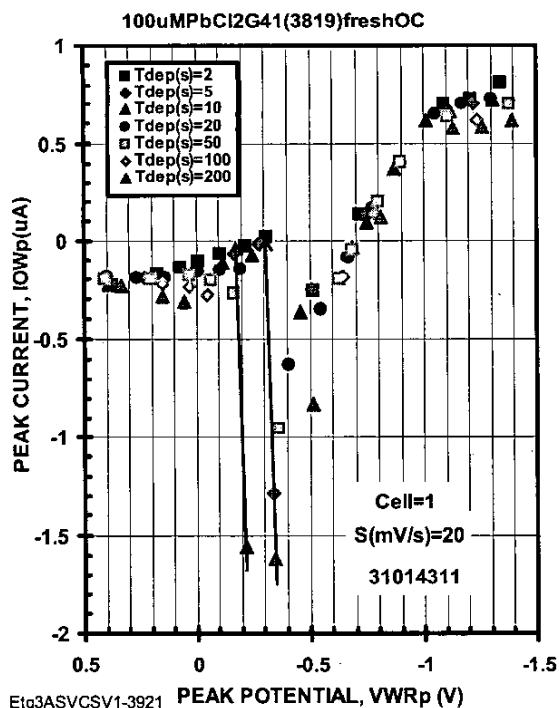
Figure 13a. 100 μM PbCl₂ ASV response.

Figure 14a. 100 μM CuSO₄ ASV response.

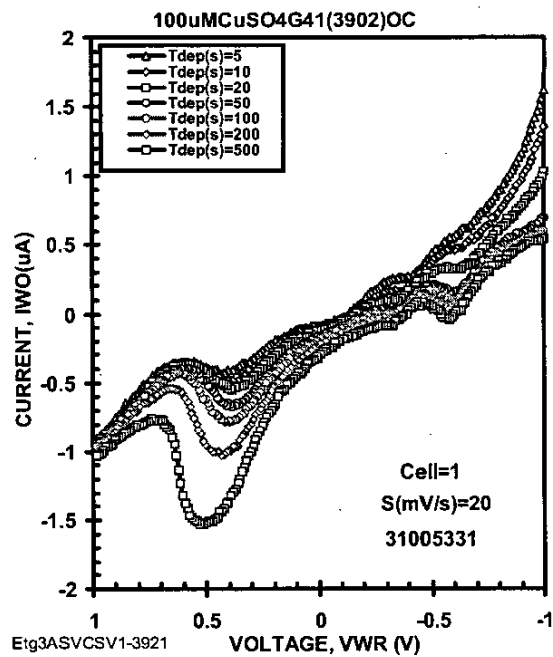Figure 13b. 100 μM PbCl₂ peak response for ASV response seen in Fig. 13a.
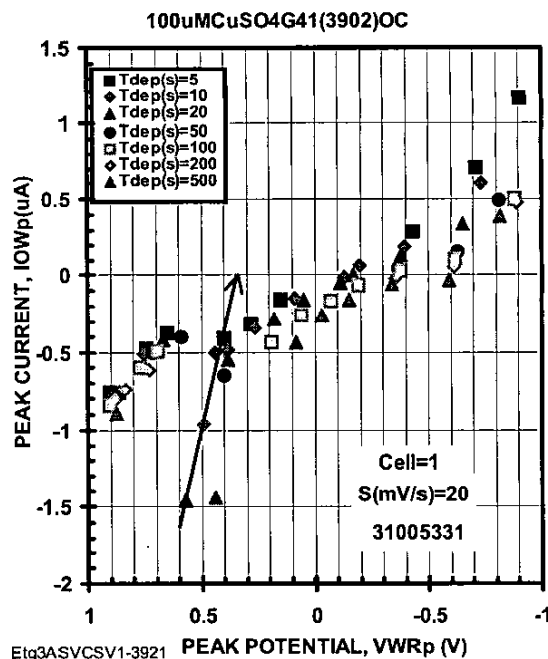

Figure 14b. 100 μM CuSO₄ peak response ASV response seen in Fig. 14a.
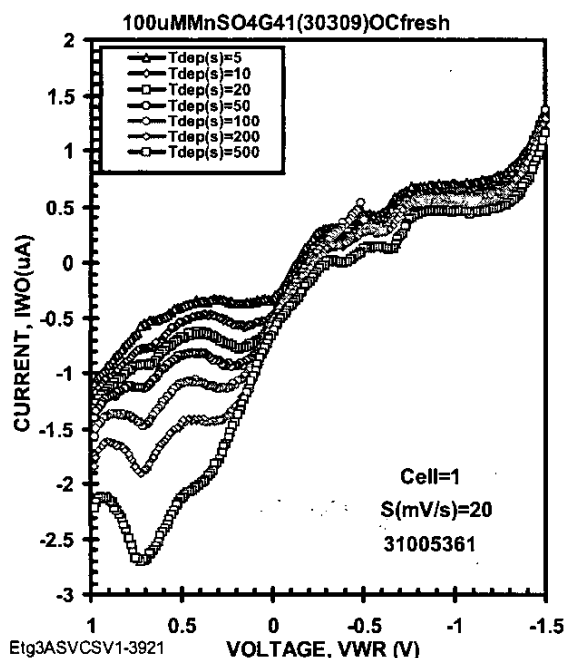
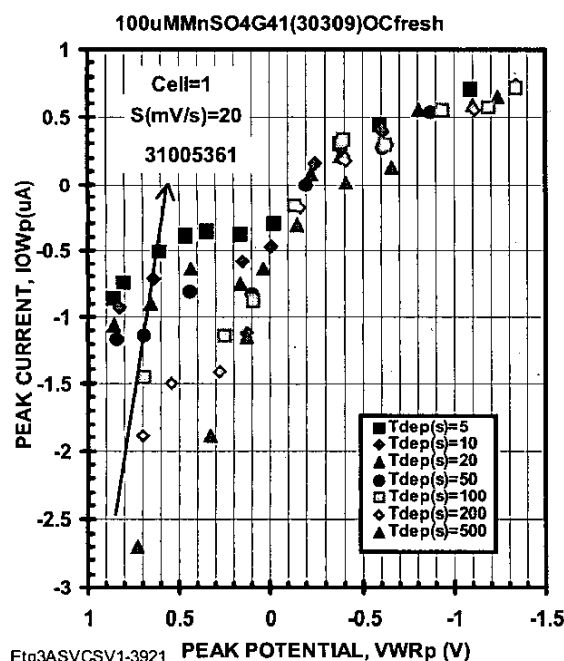f1363_8.doc - 9

371

Figure 15a. 100 μM MnSO₄ ASV response.

Figure 15b. 100 μM MnSO₄ peak response for ASV response seen in Fig. 15a.

The extrapolation procedure removes the non-idealness associated with the deposition procedure. Non-ideal conditions occur due to the build-up of deposits on the electrodes which shifts the REDOX potential. Other factors

that affect the release of ions from the WE include the non-linear electric fields associated with the our planar configuration of electrodes.

The data for cell 1 was fitted to a least squares line and the results are shown in Fig. 16. The slope is 0.98 and the offset is close to 150 mV. That is, the voltage relationship in volts is:

$$V(REDOX)_{meas} = V(REDOX)_{cal} + 0.15$$

Table 2. Oxidation reaction used to calculate E^0_{cal}.

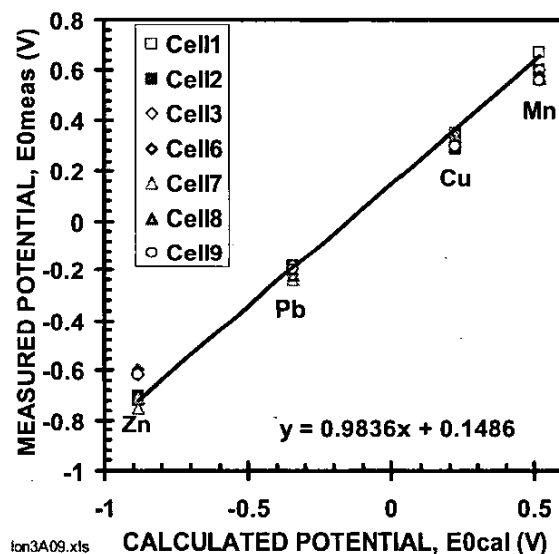| METAL	OXIDATION REACTIONS
Mn	$Mn^{2+} + 2H_2O = MnO_2 + 4H^+ + 2e^-$
	$E^0 = 1.228 - 0.1182pH - 0.0295*log(Mn^{2+})$
Cu	$Cu = Cu^{2+} + 2e^-$
	$E^0 = 0.3219 + 0.0295*log(Cu^{2+})$
Pb	$Pb + 2OH^- = PbO + H_2O + 2e^-$
	$E^0 = -0.580 - 0.059*log(OH^-)$
Zn	$Zn = Zn^{2+} + 2e^-$
	$E^0 = -0.763 + 0.0295*log(Zn^{2+})$

Figure 16. Calibration curve using Zn, Pb, Cu, and Mn. The fitted line used results from Cell 1.

The peak of the ASV curves was determined by taking the second derivative of the ASV curves seen in Figs. 12a to 15a. The REDOX potentials for seven out of nine cells are plotted in the calibration curve seen in Fig. 16. Unfortunately the response for the Mn Cells 4 and 5 were unacceptable; so all the data from these two cells was omitted from the calibration analysis. The reactions analyzed are listed in Table 2. It is seen that only the Cu and Zn exhibit simple reactions; whereas, the Mn and Pb reactions involve water or hydroxyl ions. The reactions

were analyzed for pH = 7 and for 100 µM concentrations. These values provided the calculated REDOX potential, E^0_{cal}, seen in Fig. 16.

The reference electrode used these studies was gold and has an offset potential of ~150 mV for the scan rate of 20 mV/s. This value can be compared to the potentials for reference electrodes of 318 mV for Cu-CuSO4 and 222 mV Ag-AgCl. [9, p. 66]

6.3 Scan Rate Dependence

The effect of scan rate on peak response is shown in Fig. 17 for scan rates of 10, 20, and 50 mV/s, for seven T_{dep} values ranging from 5 to 500 s, for deposition potential of E2 = -1.0 V and for the Au electrodes. The figures show that as the scan rate increases (a) the peak height increases and (b) the peak voltage moves toward more positive voltages. The peak height follows the empirical relationship [7, p. 236]:

$$Ip = 2.99 \cdot 10^5 \cdot \alpha^{1/2} \cdot A \cdot D^{1/2} \cdot C \cdot S^{1/2}$$

where α is the transfer coefficient, A the area of the WE, D the diffusion coefficient, C the concentration of the electroactive species, and S the scan rate. That is the peak height increases as the square root of the scan rate.
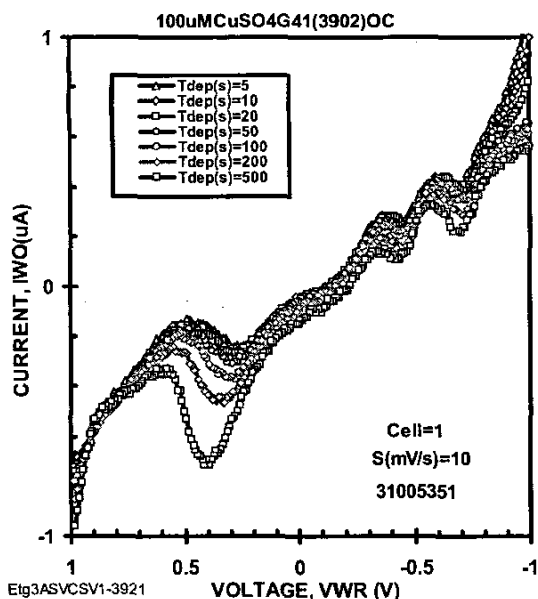

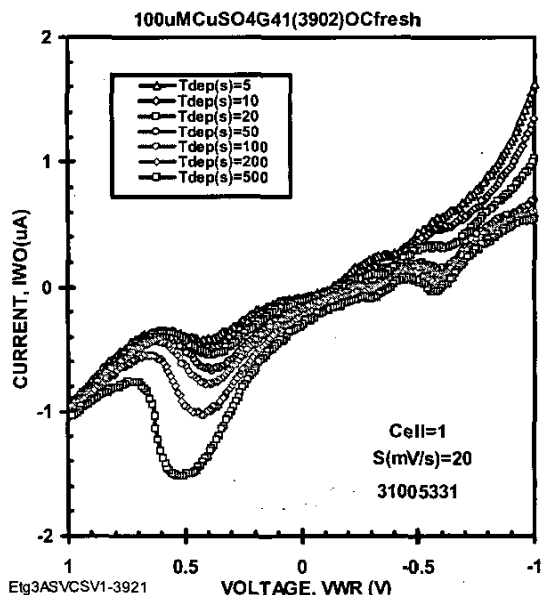Figure 17a. 100 µM CuSO4 ASV response for 10 mV/s scan rate.

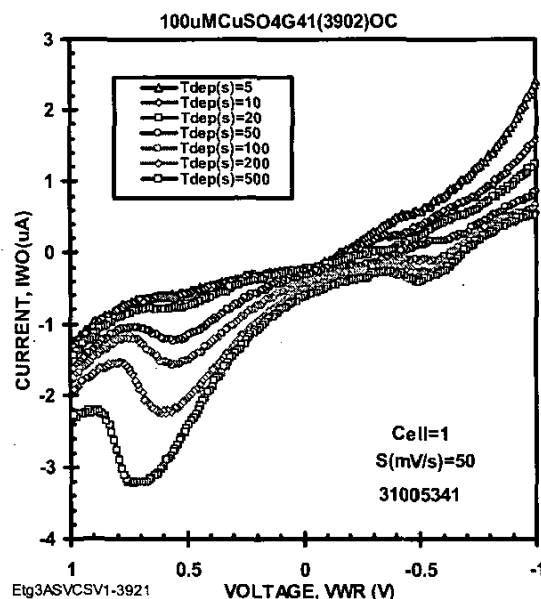Figure 17b. 100 µM CuSO4 ASV response for 20 mV/s scan rate.

Figure 17c. 100 µM CuSO4 ASV response for 50 mV/s scan rate.

The shift in the peak voltage with scan rate means that the calibration curve is scan rate dependent. From a sensing standpoint, higher scan rates generate larger peak currents; however, this can push the peak into the oxygen generation region. For our work, it has been found that a scan rate of 20 mV/s is a good compromise between the many competing factors.

6.4 Open/Closed Chamber Response

The E-Tongue 3 chamber was designed to have a cover glass that is 0.5 mm above the electrode surface. This is known as the closed chamber configuration.

Since the electrodes have an overall radius of 1.25 mm, the cover glass truncates the ion stream lines between the WE and AE. Thus, the geometry of the sensor in the closed chamber configuration is more two dimensional than in the open chamber configuration. In the open chamber configuration the cover glass is removed and this allows the use of a sample volume of 1 mL.

The volume sampled by the open chamber is assumed to be a 2.5-mm cube which is 12 µL. This follows from the 2.5-mm diameter of the electrodes. For the closed chamber, the sampled volume is 3 µL. Thus one would expect the peak height to be a factor of four small for the closed versus the open chamber.

Measurement for open and closed chambers are shown in Figs. 18a and 18b, respectively. As seen in the figures, the peak heights differ by a factor of about three. Thus, one should anticipate that the peak heights measured in the closed chamber will be smaller by at least a factor of three over open chamber measurements.
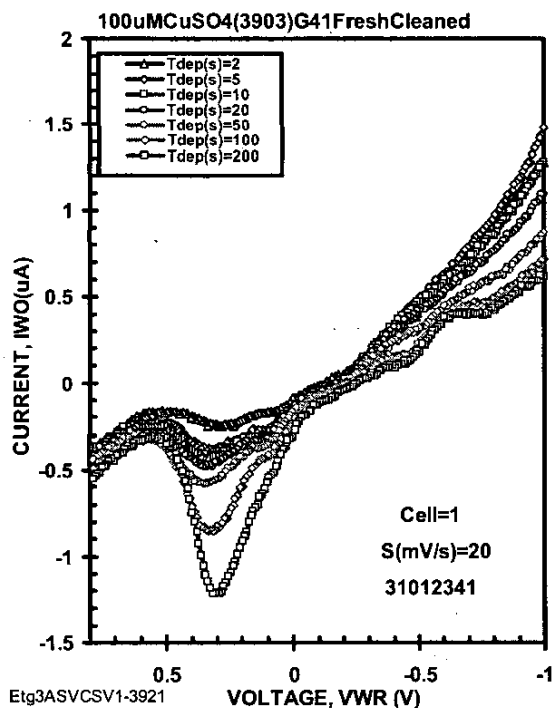

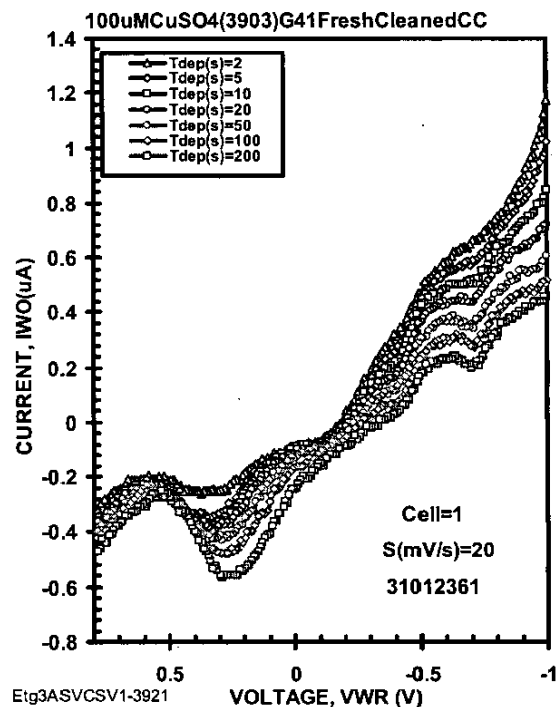Figure 18a. Open chamber ASV response for 100 µM CuSO$_4$ scanned at 20 mV/s.

Figure 18b. Closed chamber ASV response for 100 µM CuSO$_4$ scanned at 20 mV/s.

6.5 Two Species Analysis

The detection of 100 uM Cu and 100 µM Pb is shown in Figs. 19. From Fig. 19b, the REDOX potential for Cu is +0.32 V and the REDOX potential for Pb is -0.2 V. These values are consistent with the REDOX potentials for Pb and Cu shown in Figs. 16b and 17b, respectively.

The ASV response seen in Fig. 19a indicates that the peak height for Cu is small than for Pb even though both species are present in solution at the same concentration. This was observed before in Figs. 16a and 17a and in Fig. 2. Notice also that there are a number of other peaks that appear. These can be an asset in the identification of the peak system. Further work in needed to fully analyze this response.
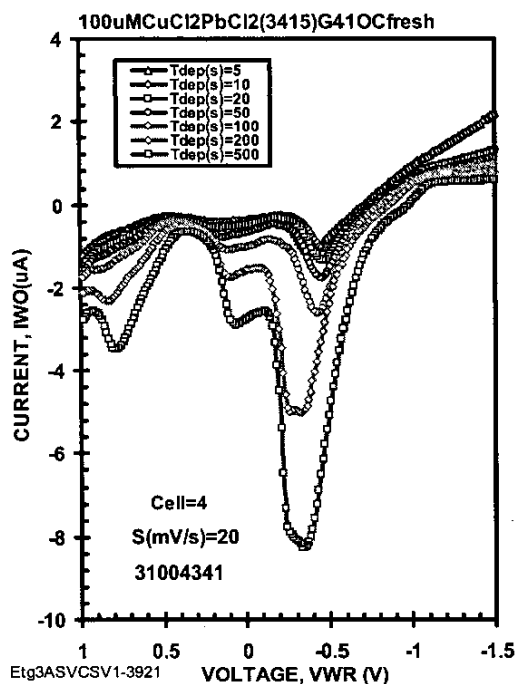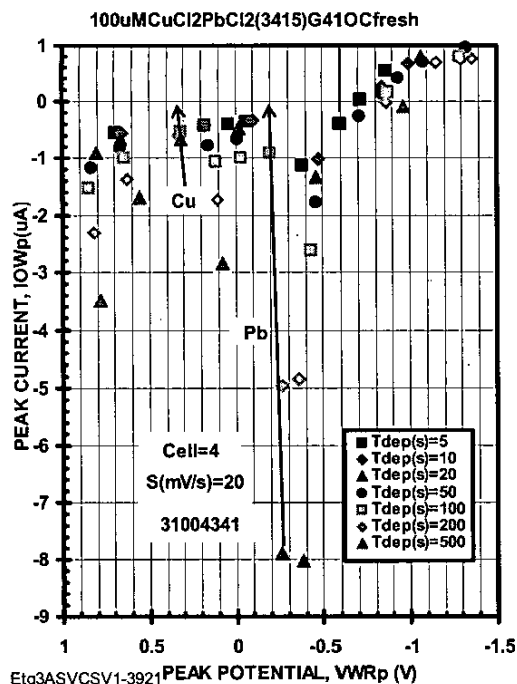
Figure 19a. Pb and Cu ASV response.

Figure 19b. Pb and Cu ASV peak response.

7   DATA ANALYSIS

The GRAMS/AI spectroscopy data processing software tools from Thermo Electron Corporation was used to compare various data extraction techniques [10].
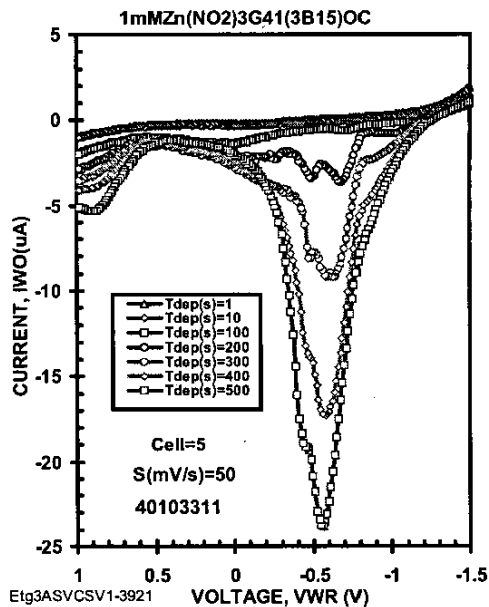

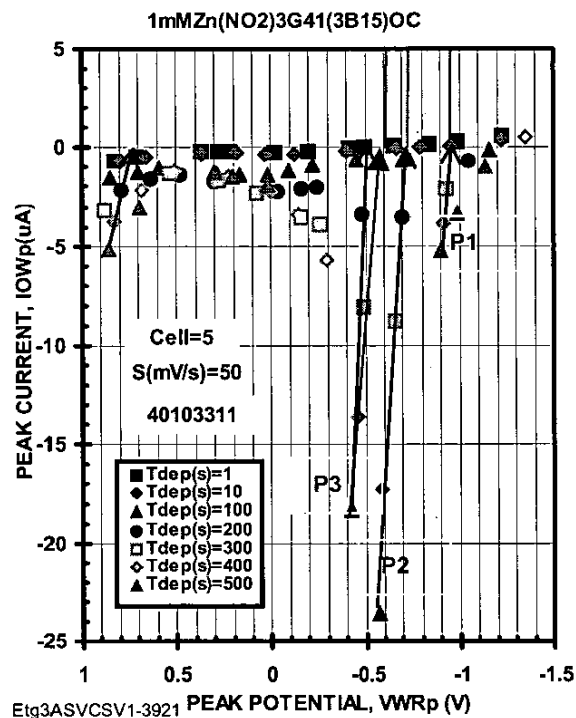Figure 20a. 1 mM $Zn(NO_2)_3$ ASV curves for data analysis.

Figure 20b. ASV peak analysis of Fig. 24a.

f1363_8.doc - 13

The GRAMS/AI software allows one to validate the peak and shoulder extraction methodology developed by JPL that is based on the Savitzky-Golay smoothing and second derivative method [11]. It also allowed an analysis of the curvature of the I-V curves obtained from the REDOX potentials to more elaborate data model such as Gaussian curve fitting and it allows the use of larger number of convolution points in order to exclude noise.
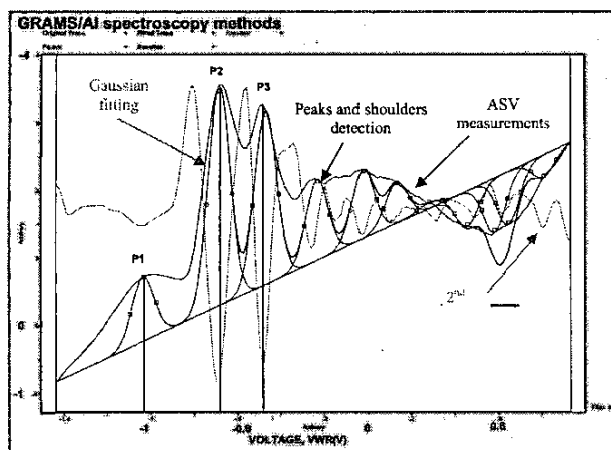

Figure 20c. Analysis for the detection of peak and shoulder in the ASV spectroscopic data seen in Fig. 24a.
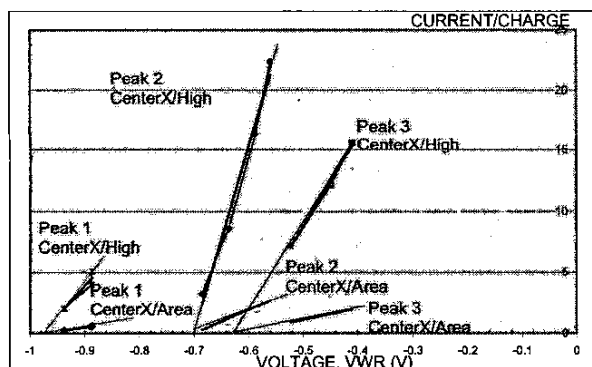

Figure 20d. Correlation of peak center, height and area for T_{dep} 200, 300, 400 and 500 s and determination of Ep_0 for the reactions by extrapolation to zero peak current.

The approach is illustrated in Fig. 20a using the experimental data of 1mM $Zn(NO_2)_3$ for a T_{dep} varying from 1 to 500 s. The JPL methodology, shown in Fig. 20b, found 3 reactions by correlating the peaks positions and peak height for different deposition times.

In Fig. 20c, the GRAMS/AI window shows the result of the peak finding algorithm. GRAM/AI finds the 3 peaks identified by the JPL method. In Fig. 20c, the red line shows the ASV curves, the blue line shows the second derivative using the Savitzky-Golay method with 7-point convolution; the green line shows the Gaussian fitting of

each identified peak; and the vertical black lines show the identification of the reactions. The GRAMS/AI software also gives the properties of each peak in terms of their center, area, and high. We correlate the center, high and area of the 3 peaks for different T_{dep} as shown Fig. 20d. By extrapolating to zero peak current, we obtain Ep_0 of the reaction as described in [1].

8   WATER QUALITY

This technology has been proposed for use on the ISS as a water quality monitor. The apparatus is seen in Fig. 21 and. Because it must operate in micro-gravity bubbles in the water stream are of concern. The apparatus has several novel features that include the use bubble traps to prevent bubbles in the water stream from reaching the sensor head.
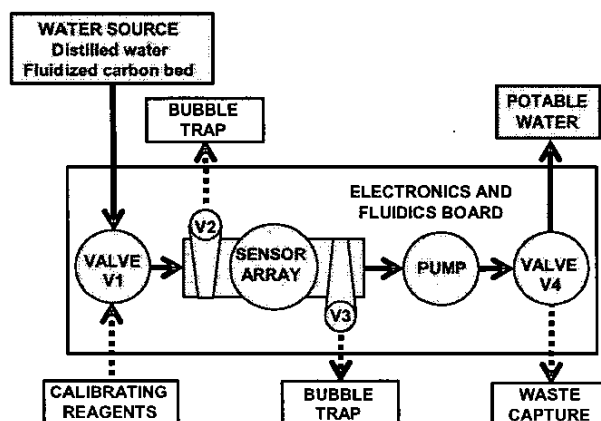

Figure 21.   Schematic view of E-Tongue prototype apparatus for use on the ISS.

The approach takes advantage of the physics where bubbles tend to form spheres and will migrate in the direction of larger openings. Thus the V-shaped features, appearing at valves V2 and V3, form the bubble trap.

Another novel feature is the fact that the apparatus does not use reagents to enhance the detection of the residual contaminates. This means that such an apparatus can be used in-line and that the water that passes through the system is potable. The only waste water generated is the occasional use of calibrating reagents and they are captured in the waste capture container.

9   DISCUSSION

This apparatus has been successfully used to characterize six metal and halide ions. The nine REDOX cells allows redundancy in the measurements so that outlier data can be identified and excluded and so that the "normal" response can be identified. Electrode cleaning procedures were found to be critical to the repeatable operation of the REDOX cells. The reference electrode used these studies

f1363_8.doc - 14

was gold which has an offset potential of ~150 mV for the scan rate of 20 mV/s. This value can be compared to the potentials for reference electrodes of 318 mV for Cu-CuSO$_4$ and 222 mV Ag-AgCl. The voltage span for the gold electrodes between the electrolysis limits is 2.5 V. This value exceeds the 1.5 V span for platinum electrodes.

In this effort we attempted to discover the limits of operation for E-Tongue 3. In that regard, we showed that the ASV peak location is scan rate dependent. In addition we showed that the closed chamber has a reduced peak height by a factor os three over the open chamber response. Finally, we showed that two compounds can be determined by measuring the ASV response for 100 µM Cu and 100 µM Pb.

A sophisticated data analysis routine was developed. The response of simple compounds (ZnSO$_4$, PbCl$_2$, CuSO$_4$, and MnSO$_4$) used in this study produced a number of reactions. The software based on taking second derivatives is able to identify the current-voltage peaks and track them to the REDOX potential by making ASV measurements at different deposition times.

10 CONCLUSION

This approach has an important role to play in the development of a reliable water quality monitor for the ISS. More work is needed in the development of data reduction algorithms that are tied to models of the reactions like those listed in Table 2 to automatically identify electroactive species. Also the software needs to be developed to control the E-Tongue system. Once a response is noted, a second experiment should be generated to further identify the species. The control system should generate a new set of measurement conditions with say different scan rates or different E1 or E2 values so as to better identify the electroactive species.

11 ACKNOWLEDGMENTS

File: AeroRedox4126Pub.doc.

12 REFERENCES

[1] M. G. Buehler, G. M. Kuhlman, D. Keymeulen, and N. V. Myung, and S. P. Kounaves, "Planar REDOX and Conductivity Sensors for ISS Water Quality Measurements" *2003 IEEE Aerospace Conference, Vol. 1, cat. No.* 02TH8593C. (March 2003).

[2] J. Wang, *Analytical Electrochemistry*, Wiley-VCH, New York, 2000.

[3] S. J. West, X. Wen, R. Geis, J. Herdan, T. Gillette, M. H. Hecht, W. Schubert, S. Grannan, S. P. Kounaves, "Electrochemistry on Mars," American Laboratory 31 (20), p. 48–, Oct. 1999

[4] Handbook of Chemistry and Physics, Electrochemical Series, No. 74, CRC Press (Boca Raton, 1994).

[5] M. G. Buehler, G. M. Kuhlman, N. V. Myung, D. Keymeulen, S. P. Kounaves, D. K. Newman and D. Lies, "Planar Array REDOX Cells and pH Sensors for ISS Water Quality and Microbe Detection", Proceedings of the International Conference on Environmental systems (ICES), Document No. 203-01-2553, Paper Offer 031ICES-216 (July 2003).

[6] R. J. Hannemann, *Semiconductor Packaging: A Multidisciplinary Approach*, J. Wiley (New York, 1994).

[7] A. J. Bard and L. R. Faulkner, *Electrochemical Methods*, 2nd Edition, Wiley & Sons (New York, 2001).

[8] R. N. Adams, *Electrochemistry at Solid Electrodes*, Marcel Dekker (New York, 1969)

[9] D. A. Jones, *Principles and Prevention of Corrosion*, Prentice Hall (Upper Saddle River, NJ, 1996).

[10] Thermo Galactic, "GRAMS/AI, User's Guide", 395 Main Street, Salem, NH 03079, USA.(http://www.thermogalactic.com).

[11] A. Savitzky and M.J.E. Golay, "Smoothing and Differentiation of Data by Simplified Least Squares Procedures", Analytical Chemistry, pp1627—1639, Vol. 36, No. 8, July 1964.

13 BIOGRAPHIES

Gregory M. Kuhlman: Greg received a B.S. degree in Bacteriology from the University of Wisconsin-Madison in 1995. Following graduation Greg has worked for the University of Wisconsin-Madison, Covance Laboratories Incorporated, and Amgen Incorporated before coming to the Jet Propulsion Laboratory (JPL) in 2000. Greg's skills include classical bacteriology techniques, modern molecular biology techniques and extensive protein chemistry skills. Greg has mastered most modern chromatographic techniques such as High Pressure Liquid Chromatography (HPLC), Fast Protein Liquid Chromatography (FPLC) and Capillary Zone Electrophoresis (CZE). As an undergraduate at the University of Wisconsin-Madison Greg worked in the lab of Dr. Eric Johnson, world renown researcher of clostridium botulinum and other food borne pathogens, and has acquired the skills for working with pathogenic microorganisms. At JPL Greg focuses his time between two groups. He works with the Planetary Protection Technologies Group where he is researching and evaluating advanced technologies for molecular detection of microbes on spacecraft materials and in spacecraft assembly facilities. Greg also works with the Microdevices Laboratory where he is utilizing his biology skill set to test and study the effects of biofilms on space flight hardware.

Didier Keymeulen received the BSEE degree from the Universite Libre de Bruxelles, Belgium, in 1987 and the MSEE and Ph.D. in Electrical Engineering and Computer Science from the Vrije Universiteit Brussels, Belgium in 1991 and 1994, respectively with the specialization in Artificial Intelligence. In 1995 he was the Belgium laureate of the Japan Society for the Promotion of Science Post Doctoral Fellowship for Foreign Researchers. In 1996 he joined the computer science division of the Japanese National Electrotechnical Laboratory as senior researcher. Since 1998, he is member of the technical staff of JPL in the Advanced Computing Technologies Group. At JPL, he is responsible for the applications of the DARPA project on evolvable hardware for adaptive computing that leads to the development of fault-tolerant electronics and autonomous and adaptive sensor technology. His expertise is in adaptive and learning hardware for autonomous systems. He is the author of over 30 papers covering topics in qualitative modeling for diagnostic and control of physical systems, adaptive and learning systems for mobile robot navigation and implementation of dynamical systems on massively parallel computers. He served as the co-chair of the NASA/DoD Workshop on Evolvable Hardware and served as its co-chair in 1999, program co-chair in 2000, and chairman in 2001. Didier is a member of the IEEE.
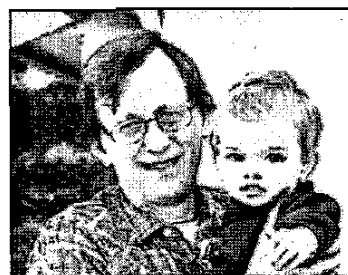
Martin G. Buehler received the BSEE and MSEE from Duke University in 1961 and 1963, respectively and the Ph.D. in EE from Stanford University in 1966 specializing in Solid State Electronics. He worked at Texas Instruments for six years, at National Bureau of Standards (now NIST) for eight years, and since 1981 has been at the Jet Propulsion Laboratory where he is a senior research scientist. At JPL he has developed p-FET radiation monitors for CRRES, Clementine, TELSTAR and STRV, E-nose which flew on STS-95, and an electrometer for the Mars '01 robot arm. Currently he serves on the staff of the New Millennium Program as a technical analyst. Martin is a member of the IEEE, Tau Beta Pi, and Sigma Nu. He holds 12 patents and has published over one hundred papers.

Samuel P. Kounaves received his BS/MS from Cal State - San Diego in 1976/78 and his Ph.D. (D.Sc.) from the University of Geneva in Switzerland in 1985. After a post-doctoral fellowships at SUNY-Buffalo and Harvard University he joined the faculty at Tufts University in 1988, where he is currently an Associate Professor of Chemistry. He has an active research group of 8 Ph.D. students and one undergraduate. He has been a principal investigator on more than 15 grants from government (NSF, EPA, DOE) and industry (PRF, EG&G, Orion). He has authored over 50 publications and holds 3 Patents. His research has been directed at the development of microfabricated electrochemical and chemically modified sensors, for use in monitoring and investigation of remote hostile environments, especially planetary bodies. Most recently he has been involved with NASA's Jet Propulsion Laboratory to include several sensor arrays for the analysis of Martian soils.

f1363_8.doc - 16